An Adaptive Mesh Semi-implicit Conservative Unsplit Method for Resistive MHD

R Samtaney[1], P Colella [2], T J Ligocki[2], D F Martin[2] and S C Jardin[1]

[1] Princeton Plasma Physics Laboratory, Princeton University, Princeton, NJ

[2] Applied Numerical Algorithms Group, NERSC Division, Lawrence Berkeley National Laboratory, Berkeley, CA

E-mail: samtaney@pppl.gov, pcolella@lbl.gov

Abstract. We present a cell-centered semi-implicit algorithm for solving the equations of single fluid resistive MHD for block structured adaptive meshes. The unsplit method [1] is extended for the ideal MHD part, and the diffusive terms are solved implicitly. The resulting second-order accurate scheme is conservative while preserving the $\nabla \cdot \mathbf{B} = 0$ constraint. Numerical results from a variety of verification tests are presented.

1. Introduction

A true description of plasma motion must rely on kinetic equations for each plasma species. As this approach is too costly for simulation of full magnetic fusion devices, a fluid description of the plasma is often used, which results from taking velocity moments of the kinetic equations describing a plasma under certain closure assumptions and the assumptions of large collisionality (see [2] for details). Magnetohydrodynamics, or MHD, is the term given to a single fluid description of a plasma in which a single velocity and pressure describe both the electrons and ions. This is distinguised from *two-fluid MHD* in which electrons and ions retain separate pressures and velocities. The simplest MHD model is that of *ideal MHD*, which ignores the diffusion terms arising from collisions, assuming that these effects are negligible compared with other terms. When these diffusion terms are retained, the mathematical model is referred to as *single-fluid resistive MHD*, which is the primary focus of this paper. While single-fluid resistive MHD may be considered to be one of the simplest models used to describe plasma dynamics, it is nonetheless rich in mathematical structure and has been successfully employed to simulate physics at the device-scale [3, 4]. We note that there have been a number of recent developments on related models in the literature that are based on further simplifications and/or incorporation of additional physical processes. An oft-used approximation of the MHD system in the presence of a strong magnetic field is to constrain the plasma compressibility in the direction perpendicular to the field. This asymptotic expansion results in simplified sets of modeling equations, and is generally referred to as *reduced MHD*. Additional processes that have been modeled are two-fluid effects including Hall term and electron pressure gradients, under the umbrella of *extended MHD* or *XMHD* [5]. In this paper, we describe a semi-implicit method for single fluid resistive compressible magnetohydrodynamics (MHD). At the heart of this method is the extension of Colella's unsplit algorithm [1] for multidimensional hyperbolic conservation laws and the recent work of Crockett et al.[6]. The outline of this paper is as follows. We first write the equations for

single fluid resistive MHD, followed by a description of the unsplit algorithm, and the implicit treatment of the diffusive fluxes. Most of the notation used here is introduced in the Chombo design document [7].

1.1. Governing Equations

The single-fluid resistive MHD equations couple the equations of hydrodynamics and resistive Maxwell's equations, and may be written in conservation form as,

$$\frac{\partial U}{\partial t} + \underbrace{\frac{\partial F_j(U)}{\partial x_j}}_{hyperbolic\ fluxes} = \underbrace{\frac{\partial \tilde{F}j(U)}{\partial x_j}}_{diffusive\ fluxes} , \tag{1}$$

where the solution vector $U \equiv U(x_i, t) = \{\rho, \rho u_i, B_i, e\}^T$, and the flux vectors $F_j(U)$ and $\tilde{F}_j(U)$ are given by

$$\begin{aligned} F_j(U) &= \left\{ \rho u_j \, , \, \rho u_i u_j + (p + \frac{1}{2} B_k B_k)\delta_{ij} - B_i B_j \, , \right. \\ &\quad \left. u_j B_i - u_i B_j \, , \, (e + p + \frac{1}{2} B_k B_k) u_i - B_i (B_k u_k) \right\}^T , \qquad (2) \\ \tilde{F}_j(U) &= \left\{ 0 \, , \, Re^{-1} \tau_{ij} \, , \, S^{-1} \left(\eta \frac{\partial B_i}{\partial x_j} - \eta \frac{\partial B_j}{\partial x_i} \right) \, , \right. \\ &\quad \left. Re^{-1} \tau_{ij} u_i + \frac{\gamma}{\gamma - 1} \frac{\kappa}{Re\ Pr} \frac{\partial T}{\partial x_j} + \frac{\eta}{S} \left(\frac{1}{2} \frac{\partial B_k B_k}{\partial x_j} - Bi \frac{\partial B_j}{\partial x_i} \right) \right\}^T . \qquad (3) \end{aligned}$$

In the above equations, ρ is the density, u_i is the velocity, B_i is the magnetic field, p and T are the pressure and temperature respectively, and e is the total energy per unit volume of the plasma. The plasma properties are the resistivity η, the thermal conductivity κ, and the viscosity μ, which have been normalized, respectively, by a reference resistivity η_R, a reference conductivity κ_R, and a reference viscosity μ_R. The ratio of specific heats is denoted by γ and taken to be $5/3$ through out this work. The non-dimensional parameters in the above equations are the Reynolds number defined as $Re \equiv \rho_0 U_0 L/\mu_R$, the Lundquist number defined as $S \equiv \mu_0 U_0 L/\eta_R$, and the Prandtl number denoted by Pr, which is the ratio of momentum to thermal diffusivity. The non-dimensionalization was carried out using the Alfvén speed $U_0 = B_0/\sqrt{\mu_0 \rho_0}$, where B_0, ρ_0, and μ_0 are the characteristic strength of the Magnetic field, a reference density and the permeability of free space, respectively, and L, a characteristic length scale. The equations are closed by the following equation of state $e = \frac{p}{\gamma - 1} + \frac{\rho}{2} u_k u_k + \frac{1}{2} B_k B_k$, The stress tensor is related to the strain as $\tau_{ij} = \mu \left(\frac{\partial u_i}{\partial x_j} + \frac{\partial u_j}{\partial x_i} \right) - \frac{2}{3} \mu \frac{\partial u_k}{\partial x_k} \delta_{ij}$. For the purposes of this paper, we will assume that the plasma properties are constant, i.e., the non-dimensional resistivity, viscosity and thermal conductivity are all unity.

Finally, a consequence of Faraday's law is that an initially divergence free magnetic field leads to a divergence free magnetic field for all times corresponding to the lack of observations of magnetic monopoles in nature. This solenoidal property is expressed as $\nabla \cdot \mathbf{B} = 0$.

2. Semi-implicit Numerical Method for Resistive MHD

In this section we describe the semi-implicit numerical method for resistive MHD. We adopt a operator-split approach in the sense that the hyperbolic fluxes are first computed using an unsplit algorithm followed by an implicit treatment of the diffusive fluxes.

2.1. Unsplit method for hyperbolic fluxes

The method developed here has its origins in Colella [1], Saltzman [8] and Crockett et al.[6]. We begin by rewriting the equation (1) as follows.

$$\frac{\partial U}{\partial t} + \sum_{d=0}^{\mathbf{D}-1} \frac{\partial F^d}{\partial x^d} = S_D \tag{4}$$

where, where $\mathbf{D}$ is the dimensionality of physical space, and S_D is the divergence of the diffusive fluxes. We define a vector of variables called the "primitive variables" $W \equiv W(U)$. In our implementation we chose $W = \{\rho\,,\, u_i, B_i\,,\, u_i,\, p(\ or\ p_t\ )\}^T$, where $p_t = p + \frac{1}{2}B_k B_k$ is the total pressure, an alternative to pressure which proves convenient for certain problems. Rewriting the equations using W in quasilinear form, we get

$$\frac{\partial W}{\partial t} + \sum_{d=0}^{\mathbf{D}-1} A^d(W)\ \frac{\partial W^d}{\partial x^d} = S'_D, \quad A^d = \nabla_U W \cdot \nabla_U F^d \cdot \nabla_W U, S'_D = \nabla_U W \cdot S_D. \tag{5}$$

A^d is a singular matrix for MHD with an eigenvector degeneracy. It may be desingularized if a source term proportional to $S\nabla \cdot \mathbf{B}$ is included. This is essentially the approach by Powell et al. [9] in which the desingularized matrix A^d has an additional eigenvalue equal to the advection speed and corresponds to an extra wave responsible for advecting away the divergence errors.

The unsplit algorithm [1] is essentially a predictor-corrector method in which face-centered and time-centered primitive variables are predicted, followed by a corrector step in which a Riemann problem is solved using the predicted values to compute a second order accurate estimate of the fluxes: $F^{n+\frac{1}{2}}_{\boldsymbol{i}+\frac{1}{2}\boldsymbol{e}^d} \approx F^d(\boldsymbol{x}_0 + (\boldsymbol{i} + \frac{1}{2}\boldsymbol{e}^d)h, t^n + \frac{1}{2}\Delta t)$. The predictor step is further divided into a normal and a transverse predictor steps. Our algorithm is outlined below.

2.1.1. Algorithm Steps

(i) Transform to primitive variables, and compute slopes $\Delta^d W_{\boldsymbol{i}}$ in each computational cell, which are subsequently limited using Van Leer slope limiting.

(ii) **Normal Predictor:** Compute the effect of the normal derivative terms and the source term on the extrapolation in space and time from cell centers to faces. In this step we split the primitive variables as follows

$$W^n_{\boldsymbol{i}} = \begin{pmatrix} \bar{W}^n_{\boldsymbol{i}} \\ B^n_{\boldsymbol{i},d} \end{pmatrix}, \tag{6}$$

For $0 \le d < \mathbf{D}$,

$$\bar{W}_{\boldsymbol{i},\pm,d} = \bar{W}^n_{\boldsymbol{i}} + \frac{1}{2}(\pm I - \frac{\Delta t}{h}\bar{A}^d_{\boldsymbol{i}})P_\pm(\Delta^d W_{\boldsymbol{i}}), \tag{7}$$

$$\bar{A}^d_{\boldsymbol{i}} = \bar{A}^d(W_{\boldsymbol{i}}), \quad P_\pm(W) = \sum_{\pm\lambda_k > 0} (l_k \cdot W) r_k,$$

$$B_{\boldsymbol{i},\pm,d} = B_{\boldsymbol{i},d}, \quad W^n_{\boldsymbol{i},\pm,d} = \begin{pmatrix} \bar{W}^n_{\boldsymbol{i},\pm,d} \\ B^n_{\boldsymbol{i},\pm,d} \end{pmatrix},$$

$$W_{\boldsymbol{i},\pm,d} = W_{\boldsymbol{i},\pm,d} + \frac{\Delta t}{2}\nabla_U W \cdot S^n_{D,\boldsymbol{i}}, \tag{8}$$

where $\bar{A}^d_{\boldsymbol{i}}$ is the matrix obtained from $A^d_{\boldsymbol{i}}$ after deleting the row and column corresponding to the normal component of the magnetic field, λ_k are eigenvalues of $\bar{A}^d_{\boldsymbol{i}}$, and l_k and r_k are the corresponding left and right eigenvectors.

Stone Correction: Crockett et al. [6] recommend the use of a correction called the "Stone Correction" to the above normal predicted states. This stems from the fact that in multidimensions the derivative of the normal component of the magnetic field in the d-direction is not zero. The Stone Correction is given as

$$\bar{W}_{\boldsymbol{i},\pm,d} = \bar{W}_{\boldsymbol{i},\pm,d} - \frac{\Delta t}{2}\left(\frac{\partial B_d}{\partial x_d}\right)_{\boldsymbol{i}} a_B, \tag{9}$$

where $a_B = \{0, B_k/\rho, u_{d_1}, u_{d_2}, -(\gamma-1)u_k B_k\}^T$, and $d_l = mod(d+l, 3)$; and the term $(\frac{\partial B_d}{\partial x_d})_{\boldsymbol{i}}$ is the derivative of the normal component of the magnetic field in the d-direction, computed using a standard second-order central difference formula.

(iii) **Transverse Predictor:** Compute estimates of F^d suitable for computing 1D flux derivatives $\frac{\partial F^d}{\partial x^d}$ using a Riemann solver. The above normal predictor step gives us left and right states at each cell interface. We employ a seven-wave linearized Riemann solver to obtain the primitive variables at the cell faces, except the normal component of the magnetic field,which is taken as the arithmetic mean of the left and right states. The entire solution vector at $\boldsymbol{i} + \frac{1}{2}\boldsymbol{e}^d$ is termed as the solution of the Riemann problem $R(.,.)$. The fluxes are then computed from the primitive variables as,

$$F^{1D}_{\boldsymbol{i}+\frac{1}{2}\boldsymbol{e}^d} \equiv F^{1D}(W_{\boldsymbol{i}+\frac{1}{2}\boldsymbol{e}^d}), \quad W^{1D}_{\boldsymbol{i}+\frac{1}{2}\boldsymbol{e}^d} \equiv R(W_{\boldsymbol{i},+,d}, W_{\boldsymbol{i}+\boldsymbol{e}^d,-,d}). \tag{10}$$

In 3D, we compute corrections to $W_{\boldsymbol{i},\pm,d}$ corresponding to one set of transverse derivatives appropriate to obtain $(1,1,1)$ diagonal coupling.

$$W_{\boldsymbol{i},\pm,d_1,d_2} = W_{\boldsymbol{i},\pm,d_1} - \frac{\Delta t}{3h}\nabla_U W \cdot (F^{1D}_{\boldsymbol{i}+\frac{1}{2}\boldsymbol{e}^{d_2}} - F^{1D}_{\boldsymbol{i}-\frac{1}{2}\boldsymbol{e}^{d_2}}) \tag{11}$$

Furthermore, in 3D, we compute fluxes corresponding to corrections made in the previous step,

$$F_{\boldsymbol{i}+\frac{1}{2}\boldsymbol{e}^{d_1},d_2} = \quad R(W_{\boldsymbol{i},+,d_1,d_2}, W_{\boldsymbol{i}+\boldsymbol{e}^{d_1},-,d_1,d_2}, d_1) \;\; d_1 \neq d_2,\; 0 \leq d_1, d_2 < \mathbf{D}. \tag{12}$$

Compute final corrections to $W_{\boldsymbol{i},\pm,d}$ due to the final transverse derivatives.

$$\begin{aligned}
2D: \quad W^{n+\frac{1}{2}}_{\boldsymbol{i},\pm,d} &= W_{\boldsymbol{i},\pm,d} - \frac{\Delta t}{2h}\nabla_U W \cdot (F^{1D}_{\boldsymbol{i}+\frac{1}{2}\boldsymbol{e}^{d_1}} - F^{1D}_{\boldsymbol{i}-\frac{1}{2}\boldsymbol{e}^{d_1}}) \\
&\quad d \neq d_1,\; 0 \leq d, d_1 < \mathbf{D}, \\
3D: \quad W^{n+\frac{1}{2}}_{\boldsymbol{i},\pm,d} &= W_{\boldsymbol{i},\pm,d} - \frac{\Delta t}{2h}\nabla_U W \cdot (F_{\boldsymbol{i}+\frac{1}{2}\boldsymbol{e}^{d_1},d_2} - F_{\boldsymbol{i}-\frac{1}{2}\boldsymbol{e}^{d_1},d_2}) \\
&\quad - \frac{\Delta t}{2h}\nabla_U W \cdot (F_{\boldsymbol{i}+\frac{1}{2}\boldsymbol{e}^{d_2},d_1} - F_{\boldsymbol{i}-\frac{1}{2}\boldsymbol{e}^{d_2},d_1}) \\
&\quad d \neq d_1 \neq d_2,\; 0 \leq d, d_1, d_2 < \mathbf{D}.
\end{aligned} \tag{13}$$

(iv) Compute final estimate of fluxes as follows. First compute the solution to the Riemann problem using the time-centered predicted states,

$$W^{n+\frac{1}{2}}_{\boldsymbol{i}+\frac{1}{2}\boldsymbol{e}^d} = \; R(W^{n+\frac{1}{2}}_{\boldsymbol{i},+,d}, W^{n+\frac{1}{2}}_{\boldsymbol{i}+\boldsymbol{e}^d,-,d}, d). \tag{14}$$

Projection: Using the normal component of the magnetic field at $\boldsymbol{i} + \frac{1}{2}\boldsymbol{e}^d$ compute a cell centered divergence. The following Poisson equation is solved using a multigrid technique with a Gauss-Seidel Red-Black ordering smoother, and a BiCGStab bottom solver.

$$\nabla^2 \chi = \sum_{d=0}^{\mathbf{D}-1} \frac{\partial B_d}{\partial x_d}_{\boldsymbol{i}} \tag{15}$$

Project the magnetic field as $B_{\boldsymbol{i}+\frac{1}{2}\boldsymbol{e}^d} = B_{\boldsymbol{i}+\frac{1}{2}\boldsymbol{e}^d} - \nabla\chi$, and replace the corrected magnetic field in to $W^{n+\frac{1}{2}}_{\boldsymbol{i}+\frac{1}{2}\boldsymbol{e}^d}$, and recompute the fluxes as $F^{n+\frac{1}{2}}_{\boldsymbol{i}+\frac{1}{2}\boldsymbol{e}^d} = F(W^{n+\frac{1}{2}}_{\boldsymbol{i}+\frac{1}{2}\boldsymbol{e}^d})$.

2.2. Implicit treatment of diffusive fluxes

At the end of the above step, the face-centered time-averaged hyperbolic fluxes have been obtained. We can update the density because the continuity equation contains no diffusion terms. The induction equation for the magnetic field is rewritten as

$$\frac{\partial B_i}{\partial t} = \mathcal{L}^B_D(B^{n+1}_i) - \nabla \cdot F^{H,n+\frac{1}{2}}_{B_i} \tag{16}$$

where $\mathcal{L}^B_D \equiv S^{-1}\frac{\partial^2}{\partial x_j \partial x_j}$, and $\nabla \cdot F^{H,n+\frac{1}{2}}_{B_i}$ is the divergence of the hyperbolic fluxes for the magnetic field components, and act as a source term in the above diffusive update step. Similarly, the momentum equation is rewritten as

$$\rho\frac{\partial u_i}{\partial t} = \mathcal{L}^u_D(u^{n+1}_i) - \nabla \cdot F^{H,n+\frac{1}{2}}_{u_i} + u_i \nabla \cdot F^{H,n+\frac{1}{2}}_{\rho} \tag{17}$$

where $\mathcal{L}^u_D \equiv Re^{-1}\frac{\partial^2}{\partial x_j \partial x_j}$, and $\nabla \cdot F^{H,n+\frac{1}{2}}_{u_i}$ is the divergence of the hyperbolic fluxes in the momentum equations, and $\nabla \cdot F^{H,n+\frac{1}{2}}_{\rho}$ is the divergence of the hyperbolic fluxes in the continuity equation. Note that the u_i multiplying $\nabla \cdot F^{H,n+\frac{1}{2}}_{\rho}$ is taken as average value of velocities at the finite volume faces obtained from the last Riemann problem solved in the hyperbolic stage.

We update the momentum and the magnetic field equations before solving the energy equation, which is rewritten as

$$\frac{\rho}{\gamma-1}\frac{\partial T}{\partial t} = \mathcal{L}^T_D(T^{n+1}) - \nabla \cdot F_e^{H,n+\frac{1}{2}} + \frac{T}{\gamma-1}\nabla \cdot F^{H,n+\frac{1}{2}}_{\rho} - \frac{1}{2}\left[\frac{\partial \rho u_k u_k}{\partial t} + \frac{\partial B_k B_k}{\partial t}\right] + \frac{\partial e_v}{\partial x_j}^{n+\frac{1}{2}} \tag{18}$$

where $\mathcal{L}^T_D \equiv (RePr)^{-1}\frac{\gamma}{\gamma-1}\frac{\partial^2}{\partial x_j \partial x_j}$, and $\nabla \cdot F_e^{H,n+\frac{1}{2}}$ is the divergence of the hyperbolic fluxes in the energy equation. The term e_v in the above equation is given by

$$\frac{\rho}{\gamma-1}e_v = S^{-1}\left(\eta\frac{\partial B_i}{\partial x_j} - \eta\frac{\partial B_j}{\partial x_i}\right) + Re^{-1}\tau_{ij}u_i. \tag{19}$$

Because the momentum and magnetic fields have been updated, all the terms in e_v are known and taken as the average of the values at time t^n and t^{n+1}. Finally the time derivatives of the kinetic and magnetic energies are determined as a simple backward difference between times t^{n+1} and t^n. Each of the implicit solves of the diffusion terms is expressed as a variable coefficient Helmholtz equation, which is solved either with a backward Euler, or a Crank-Nicholson or an implicit Runge-Kutta technique developed by Twizell et al. [10].

2.3. AMR Implementation

We now briefly describe the main issues in implementing the above algorithm using block structured adaptive meshes using the Chombo framework. Each of the blocks is surrounded by a layer of guard cells which are filled either by exchanging data from sibling meshes at the same level or by interlevel interpolation from coarse to fine meshes. In the calculation of the second order accurate hyperbolic fluxes, linear interpolation is sufficient, while the projection operation and the diffusive fluxes require a quadratic interpolation. We employ the Berger-Oliger

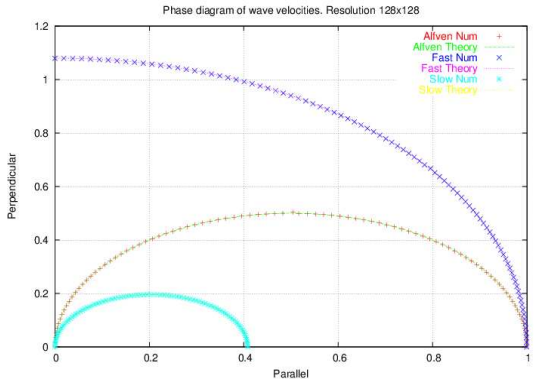

(a) Linear wave propagation of fast and slow magnentosonic, and Alfvèn waves at 45^o to the mesh. The solid curves are analytical results and symbols correspond to numerical results.

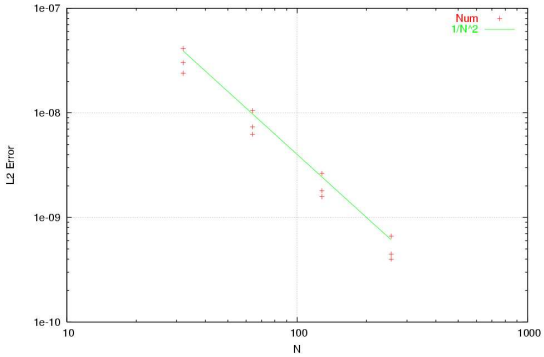

(b) L2 error between analytical and computed results for a slow magnetoscnic wave propagating at 1^o, $41^o and\ 89^o$ to the magnetic field.The solid line has a $1/N^2$ slope indicating second order convergence.

Figure 1. Linear wave propagation verification tests

.

time stepping technique in which the time steps are determined by the CFL condition imposed by the ideal MHD wave speeds and are computed at the finest level and then appropriately coarsened by the refinement ratio to determine the larger stable time step for coarser levels. We maintain flux registers which are used during synchronization when disparate levels reach the same physical time. For the hyperbolic fluxes the refluxing procedure is explicit in which coarse level fluxes at coarse fine boundaries are replaced by the sum of the fine level fluxes. The refluxing procedure for the diffusive fluxes is done implicitly, i.e., it requires a full elliptic solve on the entire mesh hierarchy. A detailed description of the implicit refluxing procedure is omitted in the interest of brevity and is similar to the method described in Martin and Colella [11].

3. Numerical Results

In this section we present results from a few verification tests.

3.1. Linear Wave Propagation

This is a test of the purely hyperbolic portion of the MHD system. In this problem, the domain is defined as the square $[0, 2] \times [0, 2]$, having periodic boundary conditions on all sides. The simulations are initialized with nearly constant initial state, with a small amplitude perturbation to setup the Alfvén, fast and slow magnetosonic waves moving obliquely at 45° to the mesh, varying the angle between the magnetic field and the wave propagation direction in the interval $[0, \pi/2]$. The results shown in 1 demonstrate that the standard phase plot of MHD wave propagation is reproduced and that the unsplit upwinding method is second-order accurate.

3.2. MHD Shock Refraction

MHD shock refraction during early stages of the Richtmyer Meshkov instability was examined in detail by Wheatley et al. [12]. An analytical solution valid in the vicinity of the quintuple point, where all the nonlinear waves intersect was obtained and compared with the numerical solution.

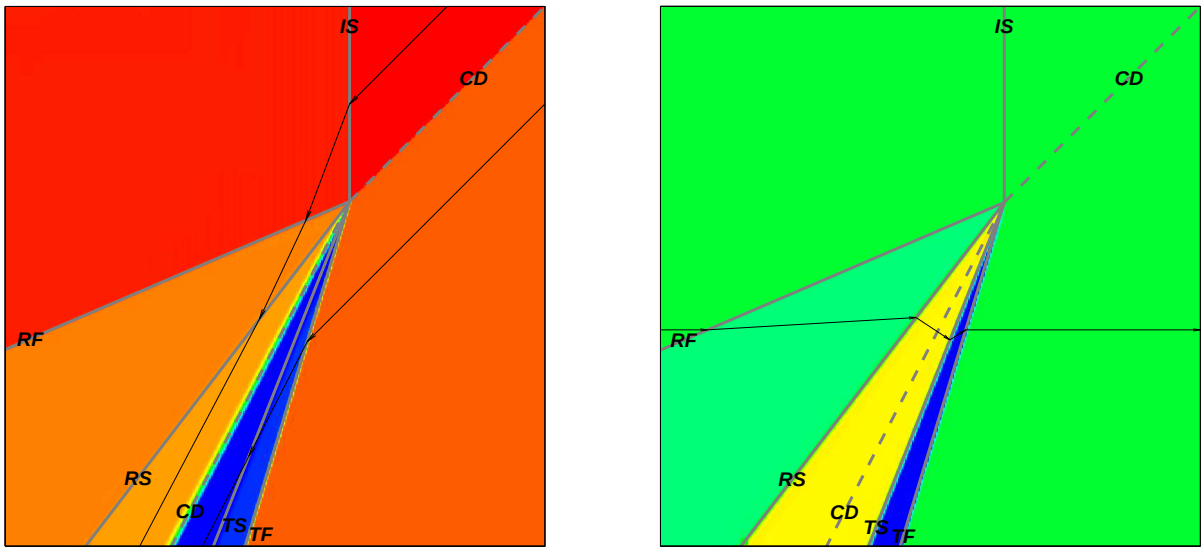

(a) Density contours

(b) B_y contours.

Figure 2. Analytical shock and contact angles for MHD shock refraction overlaid on density contours and B_y contours from the numerical results. RF and TF are fast shocks, RS is a slow shock while TS is an intermediate shock, and CD is a contact discontinuity

.

This comparison is reproduced in Figure 2 in which we observe good agreement between the analytical and the computed solution.

3.3. GEM Reconnection

Magnetic reconnection (MR) refers to the breaking and reconnecting of oppositely directed magnetic field lines in a plasma. In the process, magnetic field energy is converted to plasma kinetic and thermal energy. MR occurs in many contexts: for example, in the sawtooth-like oscillations observed in the operation of a tokamak, and in solar coronal events. In general, in magnetic reconnection, two regions are distinguished: an outer "inviscid" region and an inner "resistive" region, whose width scales with $\eta^{1/2}$, where the actual breaking and reconnecting of the magnetic field lines takes place. The initial conditions consist of a perturbed Harris sheet configuration as described in Brin et al. in [13]. This problem has been extensively studied in the literature, and because of the existence of the well-known Sweet-Parker scaling [14], we consider this a good verification test case. The domain of simulation is a 2D box $[-12.8, 12.8] \times [-6.4, 6.4]$ where the characteristic velocity scale is the Alfvén speed. The boundary conditions are periodic in the x-direction with perfectly conducting wall boundary conditions in the y-direction. In Figure 3, we plot snapshots of the components of the magnetic field at different times during the reconnection process. The reconnected flux was quantified and observed to agree with the single-fluid results presented by Brin et al. [13]. The relative timings shown in Table 1 reveal that most of the time was spent in the implicit calculation of the diffusive fluxes. The GEM reconnection problem was repeated in 3D, with large amplitude single mode perturbations in the z-direction. We observed that the reconnection process quickly transforms to that observed in 2D simulations (See Figure 4).

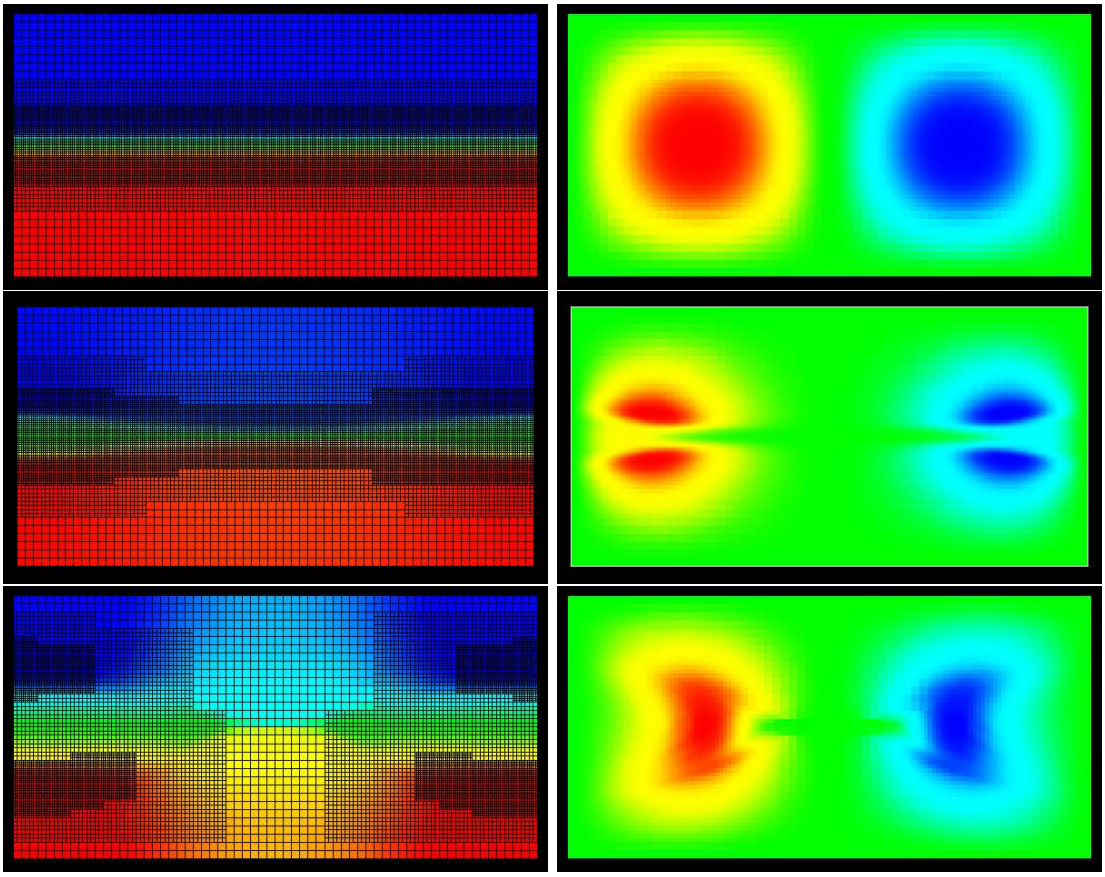

Figure 3. Magnetic reconnection in 2D (GEM reconnection challenge problem) at times $t = 0,\ 22,\ 152$. Left column: B_x with the mesh shown. Right Column: B_y.

Operation	Relative Timing
Hyperbolic Fluxes	14.70%
Parabolic Fluxes (Explicit)	0.15%
Projection	15.74%
Implicit Diffusion	61.82%
Implicit Refluxing	7.35%

Table 1. Relative timings of various operations in the semi-implicit algorithm for the GEM reconnection problem in 2D.

4. Conclusion

In this paper we presented a semi-implicit algorithm for solving single fluid resistive MHD equations on block structured adaptive meshes. The algorithm is an operator-split approach in which the hyperbolic fluxes are calculated with an extension of the Colella unsplit algorithm to MHD, and the diffusive fluxes are implicitly evaluated. The resulting scheme is conservative and preserves the solenoidal nature of the magnetic field by projection. The scheme is verified with test cases of linear wave propagation, MHD shock refraction, and magnetic reconnection.

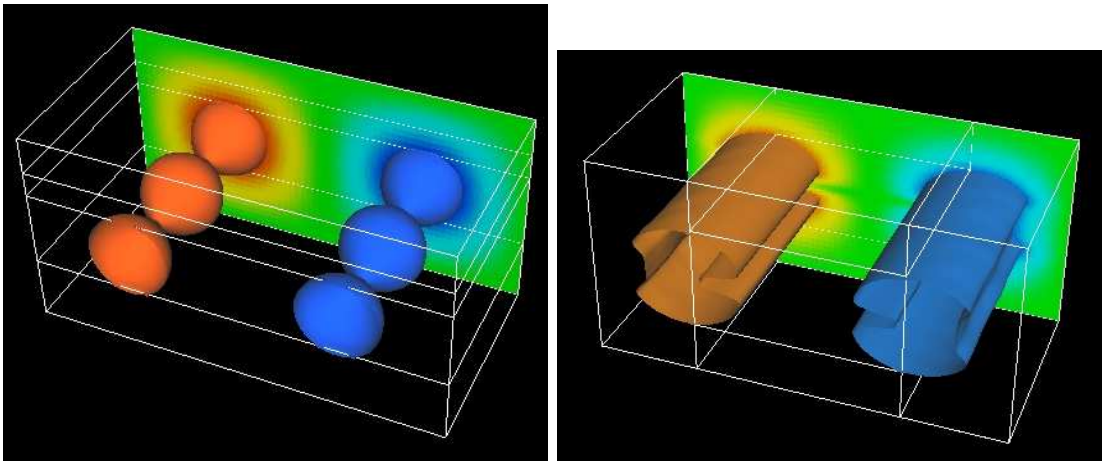

Figure 4. Magnetic reconnection in 3D. The GEM initial conditions in 2D are perturbed in the z-direction. The B_y field is shown at $t = 0$ on the left and at a later time on the right indicating an essentially 2D reconnection pattern.

Acknowledgments

This work was supported under the DOE SciDAC program (USDOE Contract no. DE-AC020-76-CH03073).

References

[1] P. Colella. Multidimensional upwind methods for hyperbolic conservation laws. *J. Comp. Phys.*, 87:171–200, 1990.

[2] R.J. Goldston and P.H. Rutherford. *Introduction to Plasma Physics.* Institute of Physics Publishing, Bristol and Philadelphia, 1997.

[3] W. Park and et al. Plasma simulation studies using multilevel physics models. *Phys. Plasmas*, 6:1796–1803, 1999.

[4] C. R. Sovinec and et al. Nonlinear magnetohydrodynamics simulation using high-order finite elements. *J. Comp. Phys.*, 195:355–386, 2003.

[5] R. D. Hazeltine and J.D. Meiss. *Plasma Confinement.* Frontiers in physics; v.86. Addison-Wesley, Redwood City, CA, 1992.

[6] R. K. Crockett, P. Colella, R. T. Fisher, R. I. Klein, and C. F. McKee. An unsplit, cell-centered Godunov method for ideal MHD. *J. Comp. Phys.*, 203:422–448, 2005.

[7] P. Colella and et al. Chombo software package for AMR applications design document.

[8] J. Saltzman. An unsplit 3d upwind method for hyperbolic conservation laws. *J. Comp. Phys.*, 115:153–168, 1994.

[9] K.G. Powell, P.L. Roe, T.J. Linde, T.I. Gombosi, and D.L. DeZeeuw. A solution-adaptive upwind scheme for ideal magnetohydrodynamics. *J. Comp. Phys.*, 154:284–300, 1999.

[10] E.H. Twizell, A.B. Gumel, and M.A. Arigu. Second-order, l_0-stable methods for the heat equation with time-dependent boundary conditions. *Advances in Computational Mathmatics*, 6:333–352, 1996.

[11] D. F. Martin and P. Colella. A cell-centered adaptive projection method for the incompressible Euler equations. *J. Comp. Phys.*, 163:271–312, 2000.

[12] V. Wheatley, D. I. Pullin, and R. Samtaney. Regular shock refraction at an oblique planar density interface in magnetohydrodynamics. *J. Fluid Mech.*, 522:179–214, 2005.

[13] J. Brin and et al. Geospace Environmental Modeling (GEM) magnetic reconnection challenge. *J. Geophys. Res.*, 106:3715–3719, 2001.

[14] D. Biskamp. *Magnetic reconnection in plasmas.* Cambridge monographs on plasma physics, third edition, 2000.